Third AO4ELT Conference - Adaptive Optics for Extremely Large Telescopes
Florence, Italy. May 2013
ISBN: 978-88-908876-0-4
DOI: 10.12839/AO4ELT3.13201

Point spread function reconstruction on the Gemini Canopus bench

Luc Gilles[1], B.Neichel[2], J.P.Véran[3] and Brent Ellerbroek[1]

[1]Thirty Meter Telescope Observatory Corporation, 1200 E. California Blvd, MC 102-8, Pasadena, CA 91125, USA

[2]Gemini Observatory, c/o AURA, Casilla 603 La Serena, Chile

[3]NRC Herzberg Institute of Astrophysics, 5171 W. Saanich Road, Victoria, BC, V9E 2E7, Canada

Abstract. This paper discusses an open loop, single-conjugate, point spread function reconstruction experiment performed with a bright calibration source and synthetic turbulence injected on the ground-level deformable mirror of the Multi Conjugate Adaptive Optics Canopus bench at Gemini South. Time histories of high-order Shack-Hartmann wavefront sensor slopes were recorded on the telemetry circular buffer, and time histories of short exposure K-band point spread functions with and without turbulence injected were recorded with the Gemini South Adaptive Optics Imager. We discuss the processing of the data and show that the long exposure background- and tip/tilt-removed turbulence image can be reconstructed at a percent level accuracy from the tip/tilt-removed de-noised wavefront sensor slope covariance matrix and from the long exposure background- and tip/tilt-removed static image. Future experiments are planned with multiple calibration sources at infinite and finite range and turbulence injected on 2 deformable mirrors, aiming at validating the recently published point spread function reconstruction algorithm [Gilles et. al. Appl. Opt. **51**, 7443 (2012)] for closed loop laser guide star multi-conjugate adaptive optics.

1. Introduction

Point spread function (PSF) knowledge is critical for any existing or proposed adaptive optics (AO) astronomical science program aiming at obtaining high angular resolution information (e.g. photometry and astrometry) [1]. A simulation model PSF reconstruction (PSFR) algorithm has recently been developed for Laser Guide Star (LGS) Multi Conjugate AO (MCAO), and has been evaluated via Monte Carlo simulations for the Thirty Meter Telescope (TMT) Narrow Field Infra Red AO System (NFIRAOS) under design [2]. The Gemini South Canopus AO bench [3,4] bears several similarities to NFIRAOS [5,6] and is thus an ideal platform to validate laser guide star (LGS) MCAO algorithms. We have undertaken an effort to validate LGS MCAO PSFR on this bench using calibration sources and artificial turbulence injected on the deformable mirrors.

A schematic of the bench taken from [3] is illustrated on Figure 1. The system was designed with 5 Shack-Hartmann wavefront sensors (WFSs) of order equal to 16 x 16, each equipped with an E2V39

80 x 80 charge-coupled device (CCD), 204 valid subapertures/WFS, 1.38arcsec pixels, 2 x 2 pixels/subaperture, 3.5e readout noise and a 1arcmin x 1arcmin X-shaped laser guide star asterism. Wavefront correctors currently consist of 2 piezoelectric deformable mirrors (DMs), one conjugate to ground (DM0), the other to an altitude of 9km (DM9). The system was designed to accommodate a third DM conjugate to an altitude of 4.5km, but that DM is currently unavailable. The actuator pitch is 5mm on DM0 and 10mm on DM9, leading to 240 controlled (unslaved) actuators on DM0 and 120 on DM9. The inter-actuator cross-coupling is 33%. Other components include a dedicated fast tip/tilt mirror, 3 natural guide star low-order WFSs, deployable science and natural guide star atmospheric dispersion compensators (ADCs) and calibration sources. The Gemini South Adaptive Optics Imager (GSAOI) consists of a 2 x 2 Hawaii-2RG (H2RG) detector array, each with 2048 x 2048 20mas pixels, providing a total science field of view of 80 arcsec x 80 arcsec. Each H2RG contains a programmable on-detector guide window (ODGW) that can be readout non-destructively and that we used in our PSFR experiments to record short exposure imagery.

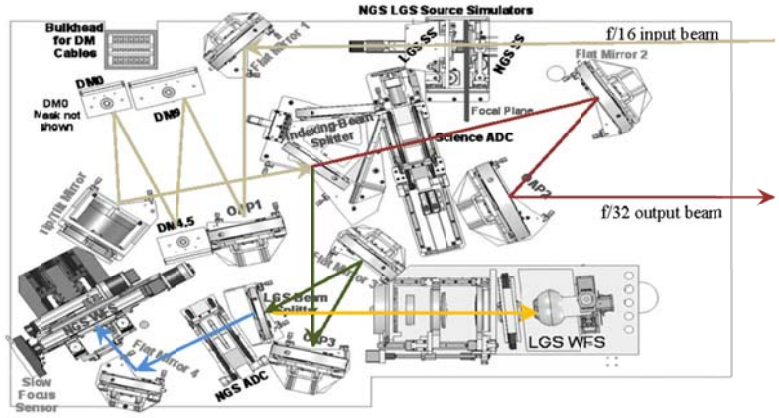

Figure 1 Schematic of the Gemini Canopus AO bench.

The paper is organized as follows. A short description of the bench experiment is provided in Section 2, the PSFR model is described in Section 3, and the processing of the data with sample PSF reconstructions are discussed in Section 4. Conclusions are drawn in Section 5.

2. Experiment description

Frozen flow Von Kárrmán turbulence was injected in closed loop on DM0 during 10s at a frame rate of 100Hz with a zero integrator gain to simulate open on loop dynamics. The injected turbulence was scaled to produce a root-mean-square (RMS) wavefront error (WFE) of 230nm. Static non-common path aberration (NCPA) commands were applied to both DM0 and DM9 concurrently with the injected turbulence to yield approximately 250nm residual NCPA WFE in addition to the 230nm turbulence WFE. A bright calibration source was used as guide star, and a time history of WFS slopes and of K-band short exposure images captured on a 16 x 16 pixel GSAOI ODGW were recorded synchronously with the DM update. We will refer to those images as “turbulence” images, keeping in mind that they are degraded by a total of ~340nm (250nm residual NCPA plus 230nm turbulence in quadrature). A time history of short exposure 24 x 24 pixel “static” images was also recorded without turbulence injected. All data is further degraded by ~8milli-arcsec (mas) 2-axis RMS tip/tilt jitter induced by the large vibration levels present on the bench.

3. Point Spread Function Reconstruction Steps

In this paper, we focus on tip/tilt-removed (TTR) PSFR, hence we removed tip/tilt at every frame from WFS slopes and from short exposure ODGW images. The latter step was implemented by correlating each short exposure image with a reference TTR diffraction limited image and Fourier shifting, which mathematically, is expressed as follows:

$$\begin{aligned} &\theta_{est} = \arg\max_{\theta} \int d^2u OTF_{DL}^{TTR}(u) OTF^{*}(u,t) e^{-2\bar{\imath}\pi u^T \theta}, \\ &OTF^{TTR}(u,t) = OTF(u,t) e^{2\bar{\imath}\pi u^T \theta_{est}}, \end{aligned} \tag{3.1}$$

where $OTF(u) = \widehat{PSF}(u) / \widehat{PSF}(0)$ denotes the optical transfer function (OTF), i.e. the Fourier transformed PSF divided by the PSF flux, and hats denote Fourier transformed quantities. The following steps were then performed:

1. Temporal averaging of the TTR short exposure turbulence and static images over 1,000 frames.
2. Temporal averaging of the TTR WFS slope covariance matrix, C_s^{TTR}.
3. Background removal (BKR) from the accumulated long exposure TTR images, which is expressed in terms of the PSF and OTF as follows:

$$\begin{aligned} &PSF_{BKR}^{TTR} = PSF^{TTR} - PSF_{BK}^{TTR}, \\ &OTF_{BKR}^{TTR} = cOTF^{TTR} + (1-c) OTF_{BK}^{TTR}, \\ &c = \widehat{PSF}^{TTR}(0) / (\widehat{PSF}^{TTR}(0) - \widehat{PSF}_{BK}^{TTR}(0)). \end{aligned} \tag{3.2}$$

   Unfortunately, PSF_{BK} was not recorded for this experiment. Instead, we estimated this quantity by least-squares fitting a plane to the boundary values of the PSF^{TTR} array.

4. Deconvolution by the ODGW pixel response function, which in Fourier space is modeled as follows:

$$\begin{aligned} &OTF^{TTR}(u) \to (\Delta\theta_{dat})^2 OTF^{TTR}(u) / \hat{d}(u), \\ &\hat{d}(u; \Delta\theta_{dat}) = (\Delta\theta_{dat})^2 \mathrm{sinc}(u_x / \Delta\theta_{dat}) \mathrm{sinc}(u_y / \Delta\theta_{dat}). \end{aligned} \tag{3.3}$$

   where $\Delta\theta_{dat} = 20$ mas is the sampling of the ODGW images.

5. OTF interpolation to (i) WFS telemetry sampling $\Delta u = \Delta x / \lambda = d_{SA} / \lambda < \Delta u_{dat}$, where $d_{SA} = 0.5$ m denotes the WFS subaperture size, $\Delta u_{dat} = 1/(n_{dat} \Delta\theta_{dat})$, and (ii) Nyquist cutoff frequency $u_c = 1/(2\Delta\theta) < u_{c,dat}$ with $\Delta\theta = \lambda/(2D) = 28.36$ mas, which leads to OTFs with $n = 2D/\Delta x = 32$ pixels, denoted as follows:

$$OTF_{tur}^{TTR}(u) = \mathrm{Interp}\left(\frac{\left[\left\langle OTF_{tur}^{TTR}(u_{tur}, t) \right\rangle_t \right]_{BKR}}{\hat{d}_{tur}(u_{tur})} \right), \quad OTF_{stat}^{TTR}(u) = \mathrm{Interp}\left(\frac{\left[\left\langle OTF_{stat}^{TTR}(u_{stat}, t) \right\rangle_t \right]_{BKR}}{\hat{d}_{stat}(u_{stat})} \right). \tag{3.4}$$

   Strehl ratio (SR) and enclosed energy (EE) are computed as follows:

$$SR = \frac{\int d^2u OTF^{TTR}(u)}{\int d^2u OTF_{DL}^{TTR}(u)}, \quad EE(\Omega) = \int d^2u OTF^{TTR}(u) \hat{d}(u; \Omega), \tag{3.5}$$

   where OTF_{DL}^{TTR} denotes the diffraction limited OTF, and $\hat{d}$ is given in (3.3).

6. Estimation of the WFS noise equivalent angle (NEA), which for a quad cell is given by:

$$\sigma_{NEA} = 1/(g_{cen}\, SNR), \tag{3.6}$$

where g_{cen} denotes the centroid gain and SNR the signal-to-noise ratio (SNR). In this experiment, $g_{cen} \sim 0.65$ /arcsec and $SNR \sim 380$, leading to $\sigma_{NEA} \sim 4$ mas.

7. Estimation of the TTR WFS "telemetry" phase covariance matrix, and subsequently structure function matrix:

$$\begin{aligned} C_{telem}^{TTR} &= (I - P_{TT})R(C_s^{TTR} - \sigma_{NEA}^2 I)R^T(I - P_{TT}^T), \\ D_{telem}^{TTR} &= \mathrm{diag}(C_{telem}^{TTR})1^T + 1\mathrm{diag}(C_{telem}^{TTR})^T - 2C_{telem}^{TTR}, \end{aligned} \tag{3.7}$$

where $I - P_{TT}$ denotes the tip/tip phase removal matrix, R the slope-to-phase reconstruction matrix (providing phase values on a grid sampled at $\Delta x = d_{SA} = 0.5$ m), which we took as in [2] to be the regularized pseudo-inverse of the WFS influence, namely

$$R = (\Gamma^T\Gamma + \xi L^T L)^{-1}\Gamma^T, \tag{3.8}$$

with $\xi = 0.25\dfrac{\max(\mathrm{eig}(\Gamma^T\Gamma))}{\max(\mathrm{eig}(L^T L))}$, and L denoting the Laplacian matrix. Note that (3.7) does not contain aliasing and fitting terms. These terms are null since turbulence was injected directly on the DMs.

8. Computation of the long exposure telemetry OTF from the phase structure function (3.7):

$$OTF_{telem}^{TTR}(u) = \frac{\int d^2x A(x)A(x+\lambda u)e^{-D_{telem}^{TTR}(x,x+\lambda u)/2}}{\int d^2x A^2(x)}. \tag{3.9}$$

9. Finally, assembling the TTR turbulence OTF estimate:

$$OTF_{tur,est}^{TTR}(u) = OTF_{telem}^{TTR}(u)OTF_{stat}^{TTR}(u)/OTF_{DL}^{TTR}(u). \tag{3.10}$$

4. Results

In this Section, we discuss the results obtained from the procedure described in Section 2. Figure 2 shows the post-processed TTR static and turbulence PSFs obtained from (3.4). The reconstructed TTR PSF as well as the absolute estimation error are displayed in Figure 3. Note the 66-fold reduction in SR error from an estimate computed without and with WFS telemetry, leading to a residual relative SR error below the percent level. Associated OTFs are displayed in Figure 4. Note that the static OTF exhibits a knee near the origin, which may indicate inaccurate background removal. Finally, Figure 5 displays the relative enclosed energy (EE) estimation error for a PSF estimate computed without and with telemetry. The estimate computed without telemetry is given by (3.10) with OTF_{telem}^{TTR} replaced by an array of all ones.

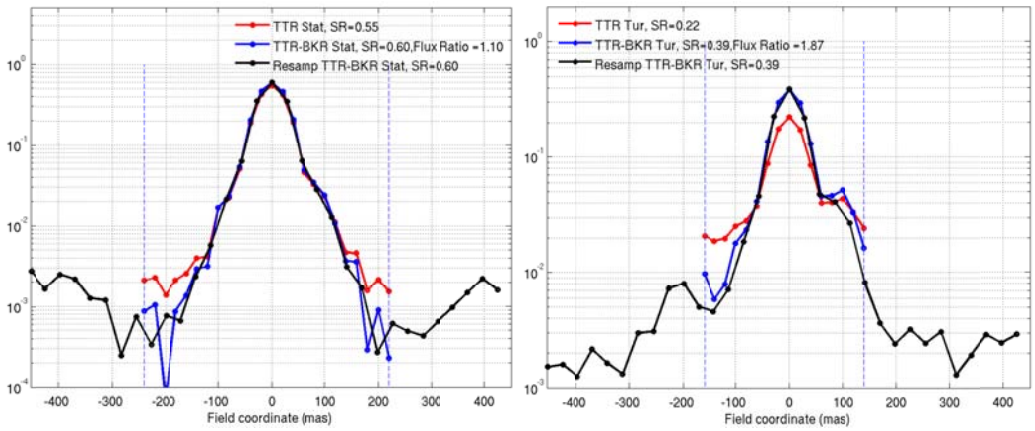

Figure 2 Static (left) and turbulence images (right). SR (PSF value at origin) is respectively 60% (250nm RMS residual NCPA) and 39% (230nm RMS injected turbulence + 250nm residual NCPA in quadrature). Red: image prior to BKR, Blue: image after BKR (note the increased SR), Black: interpolated BKR image to Nyquist rate and extrapolated to telemetry field of view (FoV) of $n\Delta\theta =$ 907.5mas. The flux ratio value reported in the legend corresponds to the parameter c defined in (3.2). Dashed vertical lines indicate the FoV of the data prior to OTF interpolation.

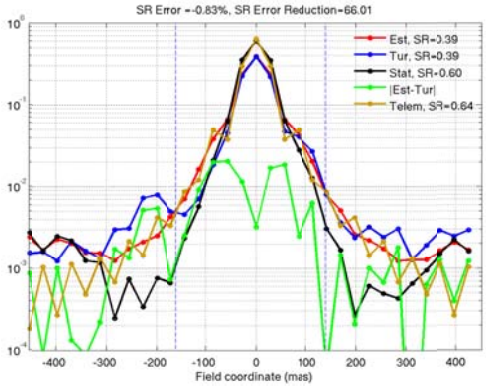

Figure 3 Red: TTR turbulence long exposure PSF estimate obtained from (3.10), Blue: truth obtained from left expression in (3.4), Black: static PSF obtained from right expression in (3.4), Green: absolute estimation error, Brown: telemetry long exposure PSF obtained from (3.9). Dashed vertical lines indicate the FoV of the turbulence data prior to OTF interpolation.

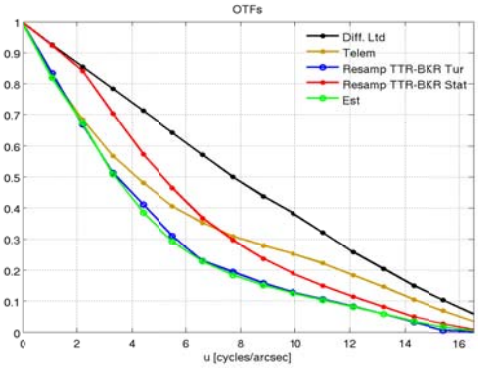

Figure 4 Black: diffraction limited OTF (denominator of (3.10)), Brown: telemetry OTF (3.9), Blue: turbulence OTF (left expression in (3.4)) , Red: static OTF (right expression in (3.4)), Green: estimated turbulence OTF (3.10).

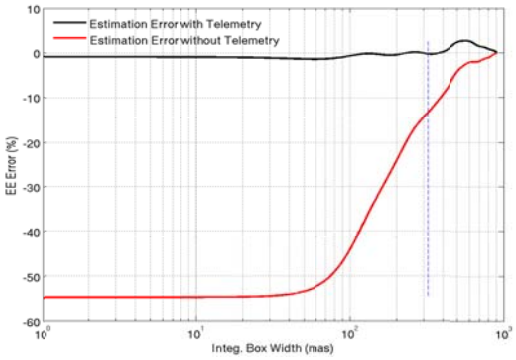

Figure 5 Black: EE estimation error for a PSF computed with WFS telemetry, Red: EE estimation error for a PSF computed without telemetry. The dashed vertical line indicates the FoV of the turbulence data prior to OTF interpolation.

5. Conclusions

Adaptive optics telemetry data from the Gemini Canopus bench is under study to validate point spread function reconstruction algorithms for laser guide star multi-conjugate adaptive optics. An initial data set with a bright on-axis calibration source and artificial turbulence injected on the ground-level deformable mirror was successfully reduced. Percent level point spread function reconstruction accuracy was achieved in K-band, corresponding to a 66-fold reconstruction accuracy improvement between point spread functions estimated without and with wavefront sensor telemetry. Data sets with multiple calibration sources at finite and infinite range and turbulence injected on two deformable mirrors will be recorded and analyzed in the near future to probe the effects of anisoplanatism and tomography.

6. Acknowledgements

The authors gratefully acknowledge the support of the TMT partner institutions. They are the Association of Canadian Universities for Research in Astronomy (ACURA), the California Institute of Technology, the University of California, the National Astronomical Observatory of Japan, the National Astronomical Observatories of China and their consortium partners, and the Department of Science and Technology of India and their supported institutes. This work was supported as well by the Gordon and Betty Moore Foundation, the Canada Foundation for Innovation, the Ontario Ministry of Research and Innovation, the National Research Council of Canada, the Natural Sciences and Engineering Research Council of Canada, the British Columbia Knowledge Development Fund, the Association of Universities for Research in Astronomy (AURA), and the U.S. National Science Foundation. L.Gilles's email address is lgilles@caltech.edu

7. References

1. R.Davies and M.Kasper, “Adaptive Optics for Astronomy”, A&A **50**, 305-351 (2012).

2. L.Gilles, C.Correia, J.P.Veran, L.Wang and B.Ellerbroek, “A simulation model based approach for long exposure atmospheric point spread function reconstruction for laser guide star multi conjugate adaptive optics”, Appl. Opt. **51**, 7443-7458 (2012).

3. M.Bec, F.Rigaut, R.Galvez et al., “The Gemini MCAO bench: system overview and lab integration,” Proc. SPIE **7015**, 701568 (2008).

4. F.Rigaut, B.Neichel, M.Boccas et al., “GeMS first on-sky results”, Proc. SPIE **8447**, 84470I-1 – 84470I-15 (2012).

5. J.Atwood, P.Byrnes, G.Herriot, J.Pazder and S.Roberts, “Optical design challenges of NFIRAOS, the First-Light Adaptive Optics System for TMT”, Proc. SPIE-OSA **7652**, 765229-1 – 765229-10 (2012).

6. J.P.Véran, E.McWeigh, D.Andersen, C.Correia, G.Herriot and J.Pazder, “The HIA MCAO laboratory bench”, Proc. SPIE **8447**, 844750-1 – 844750-12 (2012).